

# Particle alignments and shape change in $^{66}\text{Ge}$ and $^{68}\text{Ge}$

M. Hasegawa,<sup>1</sup> K. Kaneko,<sup>2</sup> and T. Mizusaki<sup>3</sup>

<sup>1</sup>Laboratory of Physics, Fukuoka Dental College, Fukuoka 814-0193, Japan

<sup>2</sup>Department of Physics, Kyushu Sangyo University, Fukuoka 813-8503, Japan

<sup>3</sup>Institute of Natural Sciences, Senshu University, Kawasaki, Kanagawa 214-8580, Japan

(Received 21 September 2004; revised manuscript received 13 December 2004; published 4 April 2005)

The structure of the  $N \approx Z$  nuclei  $^{66}\text{Ge}$  and  $^{68}\text{Ge}$  is studied by the shell model with an extended  $P + QQ$  Hamiltonian in the configuration space  $(2p_{3/2}, 1f_{5/2}, 2p_{1/2}, 1g_{9/2})$ . This framework can be shown to give a consistent and good description of energy levels, moments of inertia, and  $Q$  moments in Ge isotopes. We also investigate particle alignments and nuclear shapes in  $^{66}\text{Ge}$  and  $^{68}\text{Ge}$ . It is shown that structural changes in the four sequences of the positive- and negative-parity yrast states with even  $J$  and odd  $J$  are caused by various types of particle alignments in the  $g_{9/2}$  orbit. The nuclear shape is also investigated by calculating spectroscopic  $Q$  moments of the first and second  $2^+$  states, and the triaxiality is examined by potential energy surface.

DOI: 10.1103/PhysRevC.71.044301

PACS number(s): 21.10.Hw, 21.60.Cs, 21.10.Re

## I. INTRODUCTION

The Ge isotopes  $^{66}\text{Ge}$  and  $^{68}\text{Ge}$  have been studied intensively in experiments ([1–6] for  $^{66}\text{Ge}$  and [7–11] for  $^{68}\text{Ge}$ ) and in theoretical investigations [6,9,11–18] for many years. A thorough theoretical investigation was carried out by Petrovici *et al.* with the excited VAMPIR method for  $^{68}\text{Ge}$  [9,13–15]. The recent development of experimental techniques has accomplished detailed measurements of  $^{66}\text{Ge}$  [6] and  $^{68}\text{Ge}$  [11]. The experiments have found several bands with positive and negative parities up to high spins ( $J \leq 28$ ). A hot topic of the Ge isotopes has been the coexistence of oblate and prolate shapes [19–21] and possible  $\gamma$  softness [22,23]. The calculations based on the deformed mean field approximation in Refs. [6,21] predict oblate shapes for low-lying states of the ground-state bands of  $^{66}\text{Ge}$  and  $^{68}\text{Ge}$ , which corresponds with the prediction of the excited VAMPIR calculations for  $^{68}\text{Ge}$ . Other theoretical approaches [12,16–18], however, do not necessarily provide the same explanation as the mean field picture. The detailed data [6,11] demand to make further theoretical investigations into the structure of not only the low-energy states but the high-spin states.

We carried out shell-model calculations on a spherical basis for the  $^{64}\text{Ge}$  nucleus in a previous article [24]. The calculations with the extended  $P + QQ$  Hamiltonian [25,26] in the configuration space  $(2p_{3/2}, 1f_{5/2}, 2p_{1/2}, 1g_{9/2})$  successfully described characteristics of the structure of  $^{64}\text{Ge}$ . Moreover, for  $^{66-68}\text{Ge}$  and  $^{70}\text{Ge}$ , large-scale shell-model calculations are possible with a recent shell model code [27]. The calculations reproduce well experimentally observed energy levels and other properties of  $^{66}\text{Ge}$  and  $^{68}\text{Ge}$ . In a recent article [28], we have reported an interesting feature on the structural change of the even- $J$  positive-parity yrast states, that is, successive three bands with different types of particle alignments (including proton-neutron alignment) in the  $g_{9/2}$  orbit. We show, in this article, that similar changes are caused by various types of particle alignments in the  $g_{9/2}$  orbit, also in the other sequences of positive-parity yrast states with odd  $J$  and negative-parity yrast states with even  $J$  and odd  $J$ . Spectroscopic  $Q$  moments provide useful information about the nuclear shape and shape

change depending on the neutron number. To examine the shape and  $\gamma$  softness further, we investigate the potential energy surface (PES) in the present shell-model framework.

Section II presents parameters of the extended  $P + QQ$  Hamiltonian determined for  $^{65,66,67,68}\text{Ge}$  and energy levels obtained. In Sec. III, the shell-model results are examined in comparison with experimental and theoretical results of previous works. The focus of this article is in Secs. IV and V. In Sec. IV, various types of particle alignments are investigated in the four sequences of positive- and negative-parity yrast states with even  $J$  and odd  $J$ . Change of the first band crossing in the Ge and Zn isotopes is discussed. In Sec. V, nuclear shape and shape change are investigated. A summary is given in Sec. VI.

## II. EFFECTIVE INTERACTION AND LEVEL SCHEMES

The extended  $P + QQ$  Hamiltonian is composed of the single-particle energies, monopole corrections,  $J = 0$  and  $J = 2$  isovector pairing forces, quadrupole-quadrupole ( $QQ$ ) force and octupole-octupole ( $OO$ ) force (see Refs. [25,26] for details):

$$\begin{aligned} H = & H_{\text{sp}} + H_{\text{mc}} + H_{p_0} + H_{p_2} + H_{QQ} + H_{OO} \\ = & \sum_{\alpha} \varepsilon_{\alpha} c_{\alpha}^{\dagger} c_{\alpha} + H_{\text{mc}} - \sum_{J=0,2} \frac{1}{2} g_J \sum_{M\kappa} P_{JM1\kappa}^{\dagger} P_{JM1\kappa} \\ & - \frac{1}{2} \frac{\chi_2}{b^4} \sum_M : Q_{2M}^{\dagger} Q_{2M} : - \frac{1}{2} \frac{\chi_3}{b^6} \sum_M : O_{3M}^{\dagger} O_{3M} :, \end{aligned} \quad (1)$$

where the force strengths  $\chi_2$  and  $\chi_3$  are defined so as to have the dimension of energy by excluding the harmonic-oscillator range parameter  $b$ .

In Ref. [24] for  $^{64}\text{Ge}$ , we employed the same single-particle energies as those in Ref. [29] that are extracted from the energy levels of  $^{57}\text{Ni}$  ( $\varepsilon_{g_{9/2}} - \varepsilon_{p_{3/2}} = 3.7 \text{ MeV}$ ). However, the parameters cannot reproduce the relative energies of the positive- and negative-parity states in odd-mass Ge isotopes. We therefore lowered the  $g_{9/2}$  orbit toward the  $pf$  shell so that our shell model can reproduce experimental level schemes of

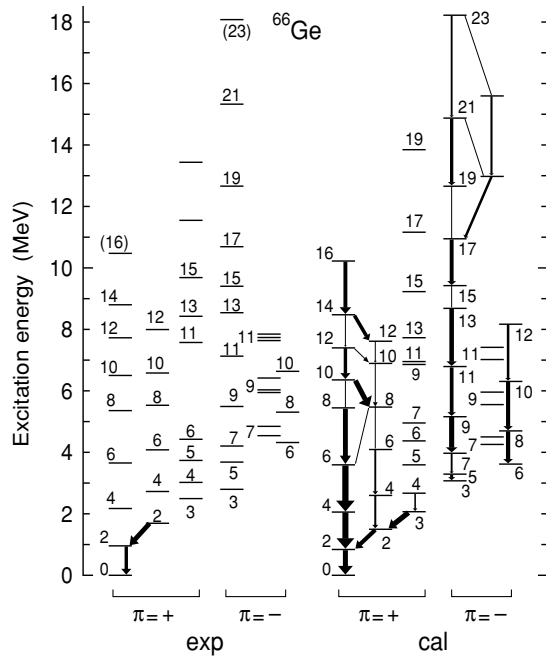


FIG. 1. Experimental and calculated energy levels of  $^{66}\text{Ge}$ . The widths of the arrows denote relative values of  $B(E2)$ .

odd-mass and even-mass Ge isotopes and also  $^{66}\text{As}$  as a whole. This was linked with the search for force strengths. We thus obtained the following set of parameters for the Ge isotopes. The single-particle energies are as follows:

$$\begin{aligned} \varepsilon_{p3/2} &= 0.00, & \varepsilon_{f5/2} &= 0.77, \\ \varepsilon_{p1/2} &= 1.11, & \varepsilon_{g9/2} &= 2.50 \quad \text{in MeV.} \end{aligned} \quad (2)$$

The value  $\varepsilon_{g9/2} = 2.5 \text{ MeV}$  coincides with that of Ref. [30]. The single-particle energies are discussed in Ref. [31]. The force strengths determined for  $^{66}\text{Ge}$  are as follows:

$$\begin{aligned} g_0 &= 0.27(64/A), & g_2 &= 0.0, \\ \chi_2 &= 0.25(64/A)^{5/3}, & \chi_3 &= 0.05(64/A)^2 \quad \text{in MeV,} \end{aligned} \quad (3)$$

with  $A = 66$ . We can get good results for  $^{68}\text{Ge}$  using the force strengths (4) with  $A = 68$ . However, somewhat better results are obtained by setting  $A = 66$  in Eq. (4) also for  $^{68}\text{Ge}$ . We therefore use the fixed force parameters [values of Eq. (4) with  $A = 66$ ] for the Ge isotopes in this article. The adopted monopole corrections are as follows:

$$\begin{aligned} H_{\text{mc}}^{T=1}(p_{3/2}, f_{5/2}) &= -0.3, & H_{\text{mc}}^{T=1}(p_{3/2}, p_{1/2}) &= -0.3, \\ H_{\text{mc}}^{T=1}(f_{5/2}, p_{1/2}) &= -0.4, & H_{\text{mc}}^{T=1}(g_{9/2}, g_{9/2}) &= -0.2, \\ H_{\text{mc}}^{T=0}(g_{9/2}, g_{9/2}) &= -0.1 \quad \text{in MeV.} \end{aligned} \quad (4)$$

Let us show energy levels of  $^{66}\text{Ge}$  and  $^{68}\text{Ge}$  calculated with the parameters (3), (4), and (4) in Figs. 1 and 2. In these figures, the calculated results excellently explain the energy levels observed in  $^{66}\text{Ge}$  and  $^{68}\text{Ge}$  [6,11], reproducing several sequences of the positive- and negative-parity states (except for a superdeformed band of  $^{68}\text{Ge}$  that is not shown in Fig. 2). For  $^{68}\text{Ge}$ , detailed band scheme was proposed from

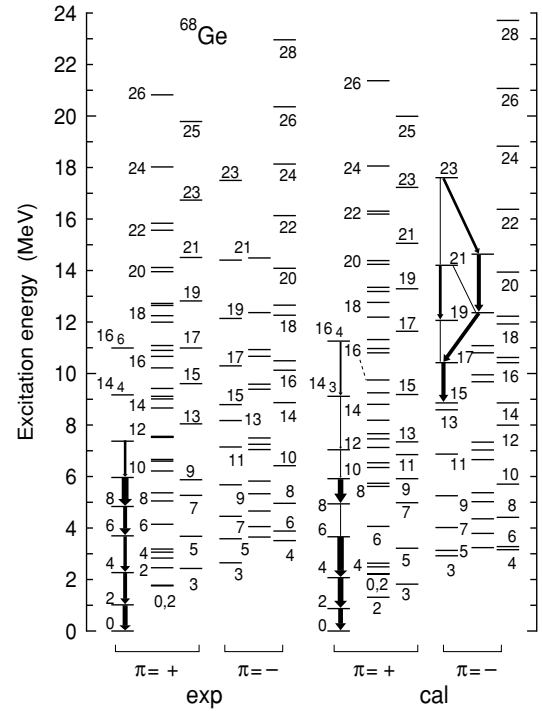


FIG. 2. Experimental and calculated energy levels of  $^{68}\text{Ge}$ . The widths of the arrows denote relative values of  $B(E2)$ .

$\Delta J = 2$  electromagnetic transitions in the experiment [11], where, for instance, the  $14_4^+$  and  $16_6^+$  states are connected to the yrast states  $8_1^+$ ,  $10_1^+$ , and  $12_1^+$ . In Fig. 2, this sequence of the states is shown in the leftmost column of the experimental results, whereas the corresponding sequence obtained by our calculations is shown in the leftmost column of the calculated results. The calculated  $14_3^+$  and  $16_4^+$  states that are connected by large  $B(E2)$  values to the yrast  $12_1^+$  state correspond well to the experimental  $14_4^+$  and  $16_6^+$  states in this figure. [Note that there are many levels with  $J^\pi = 14^+$  ( $J^\pi = 16^+$ ) near  $14_3^+$  ( $16_4^+$ ) in the calculation.] We also calculated energy levels of  $^{64}\text{Ge}$  and  $^{70}\text{Ge}$ , although high-spin states with  $J^\pi \geq 10^+$  have not been detected. Our model approximately reproduces the experimental energy levels up to  $8^+$  in  $^{64}\text{Ge}$  and  $^{70}\text{Ge}$ , as shown in Fig. 13.

Next we consider the odd-mass isotopes  $^{65}\text{Ge}$  and  $^{67}\text{Ge}$  with the above Hamiltonian, which is a severer test for the applicability of the present model. The spins of the ground states,  $3/2^-$  for  $^{65}\text{Ge}$  and  $1/2^-$  for  $^{67}\text{Ge}$ , are correctly predicted by this model as shown in Fig. 3. Moreover, the energy levels of the positive- and negative-parity states as a whole are approximately reproduced. The calculated high-spin states are somewhat pushed up as compared with the experimental ones, which may suggest further fine tuning of the parameters. However, we can see one-to-one correspondence between the experimental and calculated energy levels of  $^{65}\text{Ge}$  and  $^{67}\text{Ge}$  in Fig. 3.

Thus we can present such a consistent and good description for both the even- and odd-mass Ge isotopes, which has not been reported so far. The present extended  $P + QQ$  model can be regarded to be a reliable framework for further analysis of the structure of  $^{66}\text{Ge}$  and  $^{68}\text{Ge}$  in the following sections.

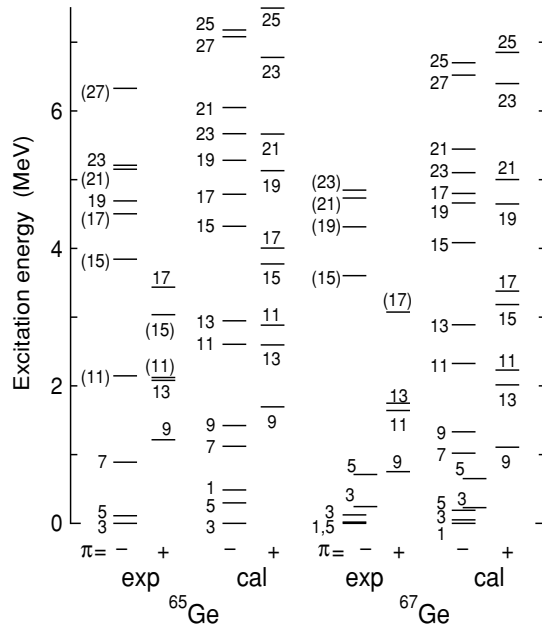


FIG. 3. Experimental and calculated energy levels of  $^{65}\text{Ge}$  and  $^{67}\text{Ge}$ . The spin of each state is denoted by the double number  $2J$ .

### III. MOMENTS OF INERTIA AND ELECTROMAGNETIC TRANSITIONS

#### A. $J$ - $\omega$ graphs

Illustrating the relation between the spin  $J$  and the rotational frequency  $\omega(J) = [E(J) - E(J - 2)]/2$  with a graph (which we call the  $J$ - $\omega$  graph) is useful in seeing the change of nuclear structure, because the moment of inertia  $J/\omega(J)$  reflects competition among various nuclear correlations.

Figure 4(a) shows the  $J$ - $\omega$  graphs for the three sequences of positive-parity states of  $^{66}\text{Ge}$ : the even- $J$  yrast states, including the ground-state (gs) band up to  $8_1^+$ ; the second band on the  $2_2^+$  state; and the odd- $J$  yrast states on the  $11_1^+$  state. The present model reproduces well the changes of the moments of inertia for these three sequences of positive-parity states. The agreement with the experimental moments of inertia is much better than that of the total Routhian surface (TRS) calculations [6] and that of the projected shell model [31].

The  $J$ - $\omega$  graph for the even- $J$  positive-parity yrast states displays a stable (collective) rotation up to  $8_1^+$  and a sharp backbending toward  $10_1^+$ . The remarkable backbending from  $8_1^+$  to  $10_1^+$  indicates a structural change. The straight line starting from  $14_1^+$  after the transitional state  $12_1^+$  is also notable. The straight line of the odd- $J$  states  $13_1^+$ ,  $15_1^+$ , and  $17_1^+$  is almost equal to that of the even- $J$  states  $14_1^+$  and  $16_1^+$ . The similar slopes suggest that these states are generated by the same rotor and the structure varies gradually. The  $J$ - $\omega$  graphs also predict structural changes at  $20_1^+$  for the even- $J$  positive-parity yrast states and at  $21_1^+$  for the odd- $J$  positive-parity yrast states.

Figure 4(b) shows the  $J$ - $\omega$  graphs for the negative-parity yrast states with odd  $J$  and even  $J$  of  $^{66}\text{Ge}$ . Our model reproduces well the change of the experimental moments of inertia except  $5_1^-$  and  $13_1^-$ , including the sharp backbending toward  $15_1^-$  where a structural change is indicated. The slope

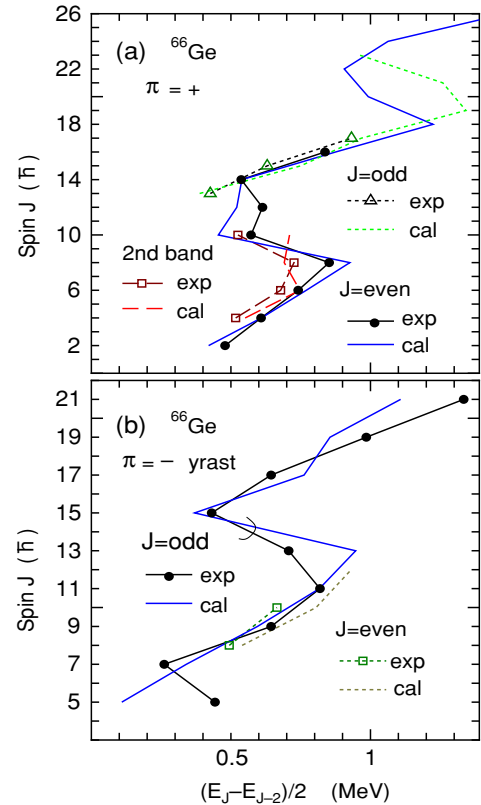


FIG. 4. (Color Online) The  $J$ - $\omega$  graphs for  $^{66}\text{Ge}$ : (a) the positive-parity yrast states with even  $J$  and odd  $J$  and the second band on  $2_2^+$ ; (b) the negative-parity yrast states with even  $J$  and odd  $J$ . For (a), the  $12_2^+$  state and the odd- $J$  states below  $11_1^+$  are omitted to avoid complexity.

for  $15_1^-$ ,  $17_1^-$ ,  $19_1^-$ , and  $21_1^-$  states is nearly equal to those of the two lines for the even- $J$  positive-parity yrast states ( $14_1^+$ ,  $16_1^+$ ) and for the odd- $J$  ones ( $13_1^+$ ,  $15_1^+$ ,  $17_1^+$ ) in Fig. 4(a). These three bands ( $15_1^- - 21_1^-$ ,  $14_1^+ - 16_1^+$ , and  $13_1^+ - 17_1^+$ ) seem to have a similar structure. Figure 4(b) also shows that the even- $J$  states  $6_1^-$ ,  $8_1^-$ , and  $10_1^-$  have a similar structure to the odd- $J$  states  $7_1^-$ ,  $9_1^-$ , and  $11_1^-$ .

We show the  $J$ - $\omega$  graphs for the positive-parity yrast states with even  $J$  and odd  $J$  of  $^{68}\text{Ge}$ , in Fig. 5(a), where the present model reproduces quite well the experimental features for  $^{68}\text{Ge}$ , except for  $17_1^+$  and  $18_1^+$ . The comparison between Figs. 4(a) and 5(a) indicates a similarity between the low-spin states up to  $6_1^+$  in the moments of inertia. There is, however, a significant difference between  $^{66}\text{Ge}$  and  $^{68}\text{Ge}$ . The backbending takes place at  $8_1^+$  in  $^{68}\text{Ge}$ , whereas it happens at  $10_1^+$  in  $^{66}\text{Ge}$ . This difference is discussed later. The theoretical  $J$ - $\omega$  graph for the states  $14_1^+$ ,  $16_1^+$ , and  $18_1^+$  of  $^{68}\text{Ge}$  is similar to the graph for the corresponding states of  $^{66}\text{Ge}$ , except the  $18_1^+$  state. The experiment [11] observed a few sets of  $14^+$ ,  $16^+$ ,  $18^+$ , and  $20^+$  belonging to different bands. The above discrepancy in the energy spacing  $E(18_1^+) - E(16_1^+)$  in Fig. 5(a) suggests a considerable interplay between these bands near  $16^+$  and  $18^+$ , which is not sufficiently taken into account in our model.

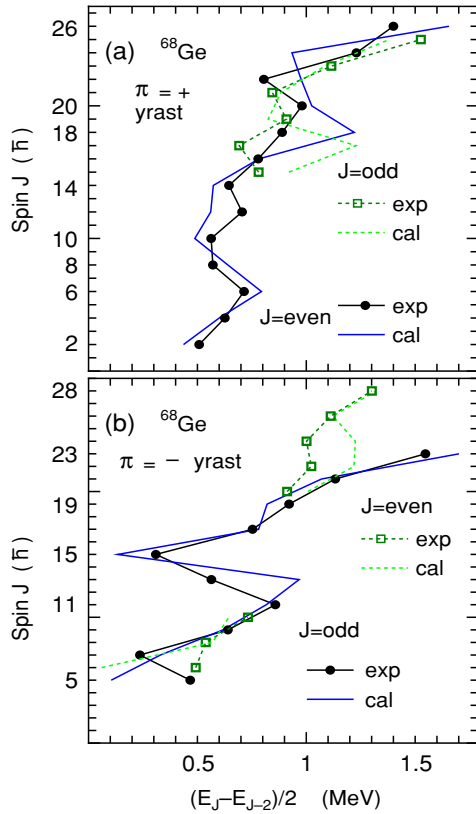


FIG. 5. (Color Online) The  $J$ - $\omega$  graphs for  $^{68}\text{Ge}$ : (a) the positive-parity yrast states with even  $J$  and odd  $J$ ; (b) the negative-parity yrast states with even  $J$  and odd  $J$ .

The  $J$ - $\omega$  graphs for the negative-parity yrast states with odd  $J$  and even  $J$  of  $^{68}\text{Ge}$  are shown in Fig. 5(b). Our model is successful in describing the change of the moments of inertia for the odd- $J$  yrast states, except for  $5_1^-$  and  $13_1^-$ . The sharp backbending toward  $15_1^-$  is finely reproduced. The low-spin band from  $5_1^-$  to  $11_1^-$  (except for the bad energy spacing between  $3_1^-$  and  $5_1^-$ ) and the high-spin sequence on  $15_1^-$  are also reproduced well. It is notable that the  $J$ - $\omega$  graph for the odd- $J$  negative-parity yrast states of  $^{68}\text{Ge}$  resembles that of  $^{66}\text{Ge}$ , which suggests a similar structure of these states in  $^{66}\text{Ge}$  and  $^{68}\text{Ge}$ .

### B. $B(E2)$ and $B(M1)$

To investigate the correspondence between experimental and calculated bands, we calculated reduced  $E2$  transition probabilities using the effective charge  $e_p = 1.5e$  for proton and  $e_n = 0.5e$  for neutron and the harmonic-oscillator range parameter  $b = A^{1/3}$ . Experimental  $B(E2)$  values [32] and some of the calculated  $B(E2)$  values are denoted by the widths of the arrows in Figs. 1 and 2 and are tabulated in Table I.

For  $^{66}\text{Ge}$ , Table I shows that the experimental large value of  $B(E2 : 2_2^+ \rightarrow 2_1^+)$  and small value of  $B(E2 : 2_2^+ \rightarrow 0_1^+)$  are qualitatively reproduced by the calculations. Although the calculated value  $281 e^2 \text{ fm}^4$  of  $B(E2 : 2_1^+ \rightarrow 0_1^+)$  is larger than the experimental one ( $190 \pm 36 e^2 \text{ fm}^4$ ), the trend of the observed  $\Delta J = 2$  transitions [6] in the two cascade bands (the

TABLE I.  $B(E2)$  values for the positive-parity yrast states and some collective states of  $^{66}\text{Ge}$  and  $^{68}\text{Ge}$ . Non-yrast states are distinguished with their subscripts from the yrast states without subscript. The subscript denotes a serial number for each spin  $J$ . The rightmost column shows the  $B(E2)$  values of Ref. [15].

$J_i^+ \rightarrow J_f^+$	$^{66}\text{Ge} (e^2 \text{ fm}^4)$		$^{68}\text{Ge} (e^2 \text{ fm}^4)$		[15]
	Exp.	Cal.	Exp.	Cal.	
$2 \rightarrow 0$	$190 \pm 36$	281	$292 \pm 33$	278	100
$4 \rightarrow 2$	$>152$	337	$229 \pm 30$	330	563
$6 \rightarrow 4$	$>19$	351	$198 \pm 66$	376	792
$8 \rightarrow 6$		275	$231 \pm 49$	0.09	291
$8_2 \rightarrow 6$		4	$198_{-198}^{+66}$	321	
$8 \rightarrow 6_2$		4	$157 \pm 33$	0.02	
$8_2 \rightarrow 6_2$		0.05	$297_{-297}^{+99}$	3.8	
$10 \rightarrow 8$	$<74$	5	$396_{-396}^{+82}$	322	852
$10_2 \rightarrow 8$		1.8	$>25$	2.7	
$10 \rightarrow 8_2$	$<206$	285		0.01	
$10_2 \rightarrow 8_2$		33	$>308$	0.25	
$12 \rightarrow 10$		191	$148_{-148}^{+66}$	49	853
$14 \rightarrow 12$		16		70	273
$14_3 \rightarrow 12$		32		42	
$16 \rightarrow 14$		219		199	672
$16_4 \rightarrow 14_3$		151		107	
$2_2 \rightarrow 0$	$1.6 \pm 0.6$	4	$2.3 \pm 0.4$	0.5	
$2_2 \rightarrow 2$	$269 \pm 127$	233	$8.0 \pm 3.5$	375	

$g_s$  band and the second positive-parity band on  $2_2^+$ ) up to  $J = 8$  can be explained by the calculated  $B(E2)$  values. The small  $B(E2 : 10_1^+ \rightarrow 8_1^+)$  value corresponds to the backbending at  $10_1^+$  seen in Fig. 4(a). This shows that the structure of the yrast states changes at  $10_1^+$  in  $^{66}\text{Ge}$ . The  $B(E2)$  values of  $10_1^+ \rightarrow 8_1^+$  and  $10_1^+ \rightarrow 8_2^+$  indicate a band crossing between  $J = 8$  and  $J = 10$ . The  $10_2^+$  state is, however, not connected to the  $8_1^+$  state, because of small  $B(E2)$ . The experimentally observed interband transition  $8_2^+ \rightarrow 8_1^+$  [32] suggests significant mixing of  $8^+$  states. Above  $10_1^+$ , the calculated  $B[E2 : J_1^+ \rightarrow (J-2)_1^+]$  values between the yrast states become quite large up to  $18_1^+$ , except  $B(E2 : 14_1^+ \rightarrow 12_1^+)$ . This explains the cascade of  $\Delta J = 2$  transitions from the tentative  $16^+$  state observed in Ref. [6]. The small value of  $B(E2 : 14_1^+ \rightarrow 12_1^+)$  corresponds to the structural change at  $14_1^+$  suggested by the  $J$ - $\omega$  graph in Fig. 4(a).

The present shell model predicts another interesting backbending at  $11_1^+$  in the sequence of the odd- $J$  positive-parity yrast states. As shown in Table II, the calculated  $B(E2 : 11_1^+ \rightarrow 9_1^+)$  value is very small, whereas  $B(E2 : \Delta J = 2)$  is large below  $9_1^+$  and above  $11_1^+$ . This shows that the sequence of the odd- $J$  positive-parity yrast states is composed of two bands, from  $3_1^+$  to  $9_1^+$  and from  $11_1^+$  to  $19^+$ . Also for the sequence of the odd- $J$  negative-parity yrast states of  $^{66}\text{Ge}$ , the  $B(E2 : 15_1^- \rightarrow 13_1^-)$  value is very small, which corresponds to the backbending at  $15_1^-$  both in the experimental and calculated  $J$ - $\omega$  graphs shown in Fig. 4(b).

The experiment for  $^{66}\text{Ge}$  [6] found a cascade of  $\Delta J = 1$  transitions connecting two  $\Delta J = 2$  sequences with even  $J$  and odd  $J$  ( $15_1^+ \rightarrow 14_1^+$  and  $13_1^+ \rightarrow 12_1^+ \rightarrow 11_1^+ \rightarrow 10_1^+$ ) and

TABLE II. Calculated  $B(E2)$  ( $e^2 \text{ fm}^4$ ) and  $B(M1)$  ( $\mu_N^2$ ) values for the positive-parity states from  $J = 9$  to  $J = 15$  of  $^{66}\text{Ge}$  and  $^{68}\text{Ge}$ . Non-yrast states are distinguished with their subscripts from the yrast states with no subscript.

$J_i^+ \rightarrow J_f^+$	$^{66}\text{Ge}$ cal.		$^{68}\text{Ge}$ cal.	
	$B(E2)$	$B(M1)$	$B(E2)$	$B(M1)$
11 $\rightarrow$ 9	0.14		1.2	
11 $\rightarrow$ 10	11	0.036	7	0.001
11 $\rightarrow$ 10 <sub>2</sub>	16	0.26	22	0.33
12 $\rightarrow$ 10	191		49	
12 $\rightarrow$ 11	22	0.66	0.5	0.14
13 $\rightarrow$ 11	312		180	
13 $\rightarrow$ 12	17	0.021	19	0.030
14 $\rightarrow$ 12	16		70	
14 $\rightarrow$ 13	23	0.003	9	0.043
14 <sub>3</sub> $\rightarrow$ 13	0.4		0.02	0.044
15 $\rightarrow$ 13	270		166	
15 $\rightarrow$ 14	3	0.015	4	0.20
15 $\rightarrow$ 14 <sub>3</sub>	12		6	0.048

supposed that the  $\Delta J = 1$  transitions are  $M1$  transitions. We calculated both  $B(E2)$  and  $B(M1)$  to examine this supposition. The results are shown in Table II. The  $B(M1)$  values obtained with our model are consistent with the results of Ref. [6] that  $B(M1 : 12_1^+ \rightarrow 11_1^+)$  is large and  $B(M1 : 13_1^+ \rightarrow 12_1^+)$  and  $B(M1 : 15_1^+ \rightarrow 14_1^+)$  are small. However, our  $B(M1 : 14_1^+ \rightarrow 13_1^+)$  value is small in contrast to the predicted staggering. Table II shows that the  $B(E2 : \Delta J = 1)$  values are not negligible for the states  $10_1^+$  to  $15_1^+$ .

For  $^{68}\text{Ge}$ , experimental  $B(E2)$  values of the  $gs$  band up to  $6_1^+$  are better reproduced by the present shell-model calculation as compared with the VAMPIR calculation as shown in Table I. Except for several band crossings, our model successfully predicts large  $E2$  transitions in the four sequences of the positive- and negative-parity states with even  $J$  and odd  $J$  deduced by cascades of  $\Delta J = 2$  transitions in Ref. [11]. Some of the calculated  $B(E2)$  values for  $8^+ \rightarrow 6^+$  transitions do not correspond with the experimental values. The small value of  $B(E2 : 8_1^+ \rightarrow 6_1^+)$  in the calculated result is in agreement with the backbending at  $8_1^+$  in Fig. 5(a), which suggests that a structural change takes place at the  $8_1^+$  state in  $^{68}\text{Ge}$ , in contrast to the backbending at  $10_1^+$  and the small value of  $B(E2 : 10_1^+ \rightarrow 8_1^+)$  in  $^{66}\text{Ge}$ . The calculation predicts a large value for  $B(E2 : 8_2^+ \rightarrow 6_1^+)$ , suggesting that the  $gs$  band up to  $6_1^+$  is connected to the  $8_2^+$  state, and a band crossing occurs between  $J = 6$  and  $J = 8$ . This is consistent with the result of the VAMPIR calculation but contradicts the result of the particle-rotor model [8], in which the  $8_3^+$  state is identified as the continuation of the  $gs$  band. We note that the sequence of the states ( $8_1^+, 10_1^+, 12_1^+, 14_4^+, 16_6^+$ ) connected by strong  $E2$  transitions in experiment corresponds well with the sequence of the states ( $8_1^+, 10_1^+, 12_1^+, 14_3^+, 16_4^+$ ) connected by large  $B(E2)$  values in theory.

The  $11_1^+$  state has not been observed experimentally in the sequence of the odd- $J$  positive-parity yrast states of  $^{68}\text{Ge}$ . Our model provides very small values for  $B(E2 : 11_1^+ \rightarrow 9_1^+)$  and

$B(E2 : 9_1^+ \rightarrow 7_1^+)$ , which suggests a structural change near the  $9_1^+$  and  $11_1^+$  states. The situation is rather complicated as compared with the backbending in other bands. To compare the  $M1$  transitions between the states from  $J = 10$  to  $J = 15$  in  $^{68}\text{Ge}$  with those in  $^{66}\text{Ge}$ , we calculated  $B(M1)$  and  $B(E2)$  values also for  $^{68}\text{Ge}$ . Table II shows that the calculated  $B(M1)$  values for these states of  $^{68}\text{Ge}$  are, up to  $14^+$ , similar to those of  $^{66}\text{Ge}$  but  $B(M1 : 15_1^+ \rightarrow 14_1^+)$  is large in  $^{68}\text{Ge}$  in contrast to  $^{66}\text{Ge}$ . Our model suggests that the  $M1$  transition could contribute to the  $\Delta J = 1$  transitions also in  $^{68}\text{Ge}$ .

For  $^{68}\text{Ge}$ , the continuation of the negative-parity states ( $17_1^-, 19_1^-, 21_1^-, 23_1^-$ ) and the termination of the odd- $J$  negative-parity band are discussed in Ref. [11]. The present shell model, which reproduces well these experimental energy levels as shown in Fig. 2, yields the following  $B(E2)$  values: 156, 234, 218, and 243 in  $e^2 \text{ fm}^4$  for the transitions  $23_1^- \rightarrow 21_2^- \rightarrow 19_2^- \rightarrow 17_1^- \rightarrow 15_1^-$ ; and 0.1, 163, and 9 in  $e^2 \text{ fm}^4$  for the transitions  $23_1^- \rightarrow 21_1^- \rightarrow 19_1^- \rightarrow 17_1^-$ . These calculated  $B(E2)$  values suggest the continuation of the states  $17_1^-, 19_2^-, 21_2^-$ , and  $23_1^-$ . This result is not consistent with the observed bands [11] but is similar to the calculated results for the  $19^-$  and  $21^-$  states of the [01,2] configuration with one  $g_{9/2}$  proton and two  $g_{9/2}$  neutrons in Ref. [11]. We note that our calculation of  $B(E2)$  values suggests the continuation of the states  $17_1^-, 19_2^-$ , and  $21_2^-$  in  $^{66}\text{Ge}$ , as shown in Fig. 1.

#### IV. PARTICLE ALIGNMENTS

Particle alignment is a key notion to understand various states of  $^{66}\text{Ge}$  and  $^{68}\text{Ge}$ . We have shown in a recent article [28] that the structural changes revealed in the  $J$ - $\omega$  graph of Fig. 4(a) can be explained by successive alignments of three combinations of nucleons in the  $g_{9/2}$  orbit: two-neutron ( $2n$ ) alignment coupled to  $T = 1, J = 8$ ; one-proton-one-neutron ( $1p1n$ ) alignment coupled to  $T = 0, J = 9$ ; two-proton-two-neutron ( $2p2n$ ) alignment coupled to  $T = 0, J = 16$ , that is,  $[(g_{9/2}^\pi)_{T=1, J=8}^2 (g_{9/2}^\nu)_{T=1, J=8}^2]_{T=0, J=16}$ .

The scenario of the changes concerning alignments for the positive-parity yrast states in  $^{66}\text{Ge}$  is as follows: (a) The  $2n$  alignment takes place at the  $8_2^+$  state. The  $2n$  aligned band crosses the  $gs$  band between  $J = 8$  and  $J = 10$ . (b) The  $1p1n$  aligned band competes with the  $2n$  aligned band near  $J = 10$  and  $J = 12$ , and there is an interplay between the two bands. (c) The  $1p1n$  alignment overwhelms the  $2n$  alignment at  $14_1^+$ , and the  $1p1n$  aligned band appears in the yrast line from  $14_1^+$  to  $18_1^+$ . (d) The  $2p2n$  aligned band takes over as the yrast state at  $20_1^+$ , continuing up to the  $26_1^+$  state where the band terminates. In the following subsections, we will see how good such a scenario concerning alignments works for various states of  $^{66}\text{Ge}$  and  $^{68}\text{Ge}$ .

##### A. Particle alignments in the even- $J$ positive-parity yrast states for $^{68}\text{Ge}$

Let us show the results for the even- $J$  positive-parity states of  $^{68}\text{Ge}$  (for  $^{66}\text{Ge}$ , see Ref. [28]). We illustrate the changes of the proton and neutron occupation numbers in the  $g_{9/2}$  orbit

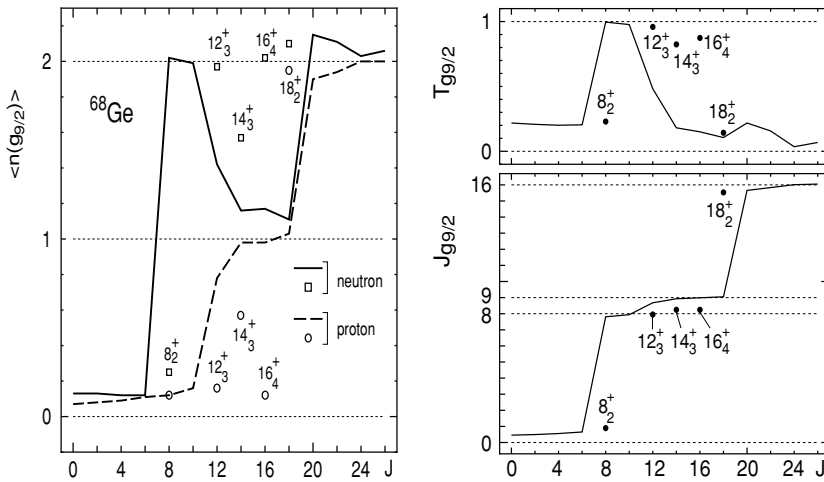


FIG. 6. (Left) The neutron and proton occupation numbers in the  $g_{9/2}$  orbit ( $\langle n_{g_{9/2}}^v \rangle$  and  $\langle n_{g_{9/2}}^\pi \rangle$ ) for the even- $J$  positive-parity yrast states (lines) and some other states (symbols) of  $^{68}\text{Ge}$ . (Right) The expectation values of the spin and isospin of nucleons in the  $g_{9/2}$  orbit ( $J_{g_{9/2}}$  and  $T_{g_{9/2}}$ ) for the even- $J$  positive-parity yrast states (lines) and some other states (symbols) of  $^{68}\text{Ge}$ .

$\langle n_{g_{9/2}}^\pi \rangle$  and  $\langle n_{g_{9/2}}^v \rangle$  and also expectation values of the spin and isospin of nucleons in the  $g_{9/2}$  orbit, which are denoted by  $J_{g_{9/2}}$  and  $T_{g_{9/2}}$ , in Fig. 6. Here, we evaluate the spin  $J_{g_{9/2}}$  and the isospin  $T_{g_{9/2}}$  as follows:  $J_{g_{9/2}} = [(\langle \hat{j}_{g_{9/2}} \rangle^2) + 1/4]^{1/2} - 1/2$  and  $T_{g_{9/2}} = [(\langle \hat{t}_{g_{9/2}} \rangle^2) + 1/4]^{1/2} - 1/2$ , where  $\hat{j}_{g_{9/2}}$  and  $\hat{t}_{g_{9/2}}$  are the spin and isospin operators of the  $g_{9/2}$  orbit.

Figure 6 narrates a scenario similar to that mentioned above for  $^{66}\text{Ge}$ . However, a spin at which  $2n$  aligned band becomes yrast is different. In  $^{68}\text{Ge}$ , whereas the  $gs$  band continues to the  $8_2^+$  state, the  $2n$  aligned band crosses the  $gs$  band before  $J = 8$ . The band crossing is also indicated by the abrupt change of the calculated  $Q$  moment at  $8_1^+$ . The  $Q$  moment is between  $-7$  and  $-13 e \text{ fm}^2$  for the  $gs$  band ( $2_1^+ - 6_1^+, 8_2^+$ ) but is  $-64$  ( $-70$ )  $e \text{ fm}^2$  for the  $8_1^+$  ( $10_1^+$ ) state. The yrast states  $8_1^+$  and  $10_1^+$  are members of the  $2n$  aligned band. Passing the transitional state  $12_1^+$ , the  $1p1n$  aligned band appears in the yrast line of  $14_1^+, 16_1^+, 18_1^+$  like  $^{66}\text{Ge}$ . There seems to be strong coupling between the  $2n$  and  $1p1n$  aligned bands at  $J = 12$ . The third band crossing takes place between  $J = 18$  and  $J = 20$ . The  $2p2n$  aligned band takes the lowest position from  $20_1^+$  to  $26_1^+$ . Figure 6 shows that the aligned nucleons in the  $g_{9/2}$  orbit couple to  $T = 1, J = 8$  in the  $2n$  aligned band ( $8_1^+, 10_1^+$ ),  $T = 0, J = 9$  in the  $1p1n$  aligned band ( $14_1^+, 16_1^+, 18_1^+$ ) and  $T = 0, J = 16$  in the  $2p2n$  aligned band ( $20_1^+, 22_1^+, \dots, 26_1^+$ ).

In Fig. 7, we illustrate the successive four bands with a graph of excitation energy versus spin  $J$ , which we hereafter call the  $E_x$ - $J$  graph. The correspondence between theory and experiment is good for the non-yrast states as well as the yrast states. However, the  $12_1^+$  state is assigned as the  $J = 12$  member of the band on  $8_1^+$  in the experiment [11], whereas the  $12_1^+$  state resembles the  $1p1n$  aligned state rather than the  $2n$  aligned state in our calculation. The  $J$ - $\omega$  graph for the even- $J$  positive-parity yrast states of  $^{68}\text{Ge}$  [Fig. 5(a)] shows an insufficient description of the energy difference  $E(18_1^+) - E(16_1^+)$ . Moreover, the calculated  $B(E2)$  values between different bands do not necessarily agree with the experimental  $B(E2)$  values in Table I. These discrepancies reveal missing correlations in our model Hamiltonian and suggest stronger interplays between the different bands near the band crossings. Although there is such an insufficiency,

the calculated  $J$ - $\omega$  graph in Fig. 5(a) and the  $E_x$ - $J$  graph in Fig. 7 as a whole trace the trends of the experimental graphs. We can attribute the changes in these graphs to the successive band crossings indicated in Fig. 6.

### B. Mechanism of particle alignments

So far, we have used the word *alignment* for the maximum angular momentum coupling in the  $g_{9/2}$  orbit. How is the angular momentum coupling of the aligned particles in the  $g_{9/2}$  orbit with the central system excluding the  $g_{9/2}$  particles? We calculated expectation values of the spin and isospin of the central system which is represented by nucleons in the  $pf$  shell ( $2p_{3/2}, 1f_{5/2}, 2p_{1/2}$ ). We denote these expectation values as  $J_{pf}$  and  $T_{pf}$  and evaluate them using the relations  $J_{pf} = [(\langle \hat{j}_{pf} \rangle^2) + 1/4]^{1/2} - 1/2$  and  $T_{pf} = [(\langle \hat{t}_{pf} \rangle^2) + 1/4]^{1/2} - 1/2$ , where  $\hat{j}_{pf}$  and  $\hat{t}_{pf}$  mean the spin and isospin operators for the subspace ( $2p_{3/2}, 1f_{5/2}, 2p_{1/2}$ ). Calculated  $J_{pf}$  and  $T_{pf}$  together with  $J_{g_{9/2}}$  and  $T_{g_{9/2}}$  are shown in Fig. 8.

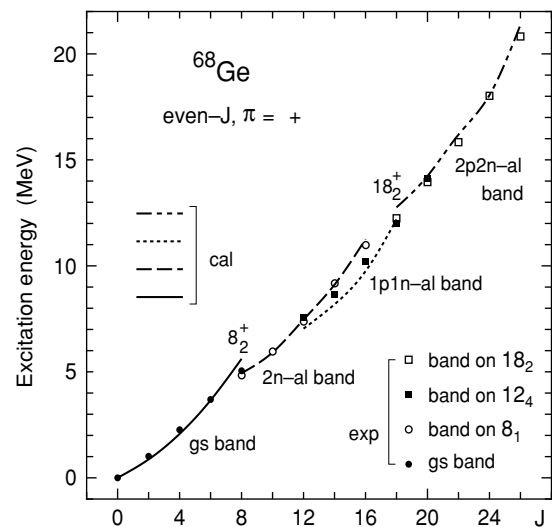


FIG. 7. Comparison of the calculated four bands with the experimentally observed bands for  $^{68}\text{Ge}$ .

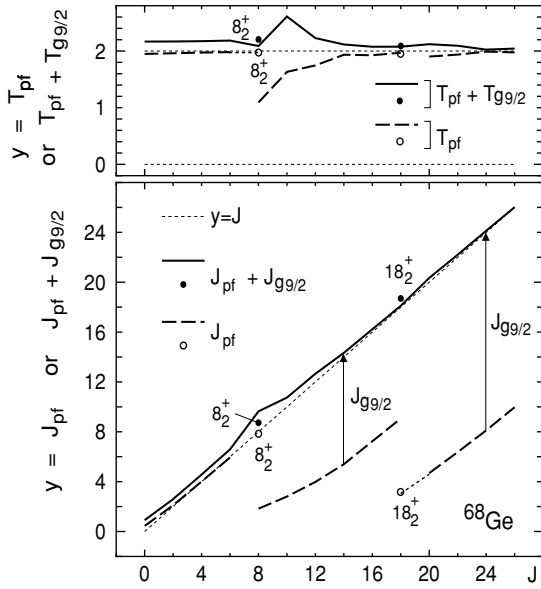


FIG. 8. The expectation values of spins  $J_{pf}$  and  $J_{g_{9/2}}$ , and those of isospins  $T_{pf}$  and  $T_{g_{9/2}}$ , for the even- $J$  positive-parity yrast states (lines) and some other states (symbols) of  $^{68}\text{Ge}$ .

Figure 8 indicates that the spin of the aligned particles in the  $g_{9/2}$  orbit actually aligns with the spin of the central system in the  $2n$ ,  $1p1n$ , and  $2p2n$  aligned bands. This situation can be called a system composed of a rotor and particles. We can see some deviation from the weak coupling of the rotor and particles near  $J = 8$  in Fig. 8. The upper panel of Fig. 8 indicates vector coupling of the isospins  $T_{pf}$  and  $T_{g_{9/2}}$  for the  $2n$  aligned yrast states with  $T = 1$ ,  $8_1^+$  and  $10_1^+$ . It should be noticed that the residual nucleons in the  $pf$  shell coupled with the aligned  $1p1n$  pair with  $T = 0$ ,  $J = 9$  must have the isospin  $T = 2$  for the nucleus  $^{68}\text{Ge}$ , whereas the residual nucleons coupled with the aligned  $2n$  pair with  $T = 1$ ,  $J = 8$  can have the isospins  $T = 1, 2$ , and  $3$ . This effect is seen in the upper panel of Fig. 8. The different isospin couplings bring about different properties to the  $1p1n$  and  $2n$  aligned bands. The problem is related to the competition between the  $T = 1$  and  $T = 0$  pair correlations in the central system.

The superiority of the  $J = 9$ ,  $T = 0$   $1p1n$  pair in the  $14_1^+$ ,  $16_1^+$ , and  $18_1^+$  states can be attributed to the condition that the  $T = 0$ ,  $J = 9$   $pn$  interaction is stronger than the  $T = 1$ ,  $J = 8$  interaction. Note that, whereas the  $T = 1$ ,  $J = 2j - 1$  interaction is repulsive, the  $T = 0$ ,  $J = 2j$  interaction is very attractive in ordinary effective interactions. If we set  $\langle (g_{9/2})^2 | V | (g_{9/2})^2 : T = 0, J = 9 \rangle$  zero, the  $1p1n$  aligned states do not become the yrast states, whereas the  $gs$  band is hardly disturbed.

What conditions cause such a nearly pure  $1p1n$  alignment? In Ref. [33], we investigated even-mass Ru isotopes around  $^{90}\text{Ru}$  which is symmetrical to  $^{66}\text{Ge}$  with respect to the particle-hole transformation in the  $(p_{3/2}, f_{5/2}, p_{1/2}, g_{9/2})$  space. We did not find any sign of the  $T = 0$   $1p1n$  alignment there and could not see a pure  $2n$  alignment at the backbending state  $8_1^+$  in  $^{90}\text{Ru}$ . A difference is that the Fermi level lies at the  $g_{9/2}$  orbit itself in the Ru isotopes but considerably far from the

$g_{9/2}$  orbit in the Ge isotopes. The appearance of the nearly pure  $2n$  and  $1p1n$  alignments in  $^{66}\text{Ge}$  and  $^{68}\text{Ge}$  is based on the condition that the high-spin orbit  $g_{9/2}$  is quite apart from the Fermi level and has the opposite parity to the  $pf$  shell, which means that excitations from  $pf$  to  $g_{9/2}$  are allowed if the number of excited nucleons is even. Therefore, we can expect the  $T = 0$   $1p1n$  alignment in  $N \approx Z$  even-even nuclei near the Ge isotopes.

We explored other nuclei  $^{64}\text{Ge}$ ,  $^{70}\text{Ge}$ ,  $^{60-68}\text{Zn}$ , and  $^{68}\text{Se}$  for the  $T = 0$   $1p1n$  aligned states, using the same shell-model interaction. The calculation for  $^{64}\text{Ge}$  predicts that the  $1p1n$  alignment takes place at  $12_1^+$  just above the  $gs$  band from  $0_1^+$  to  $10_1^+$  and continues up to  $18_1^+$ , but there is no  $2n$  aligned state in the even- $J$  positive-parity yrast states. For  $^{70}\text{Ge}$ , conversely, the calculation yields only one  $1p1n$  aligned yrast state,  $16_1^+$ . The results suggest that the  $1p1n$  aligned state is favored when the neutron excess  $N - Z$  is small, especially when  $N = Z$ . This is probably related to the existence of suitable low-energy states in the  $A - 2$  subsystem, excluding the  $1p1n$  pair  $(g_{9/2})^2_{J=9, T=0}$ , for instance, such as the  $T = 0$  states of  $^{62}\text{Ga}$  for  $^{64}\text{Ge}$  and the  $T = 1$  states of  $^{64}\text{Ga}$  for  $^{66}\text{Ge}$ . We got the  $T = 0$   $1p1n$  aligned states  $14_1^+$  and  $16_1^+$  above the  $gs$  band ( $0_1^+ - 10_1^+$ ) for  $^{62}\text{Zn}$ , whereas we have no  $1p1n$  aligned state in the even- $J$  positive-parity yrast states for the Zn isotopes with  $A > 62$ . The  $^{68}\text{Se}$  nucleus has the maximum dimension in the present shell-model calculations, that is, about  $1.6 \times 10^8$  for  $0_1^+$ . The calculation predicts the  $T = 0$   $1p1n$  alignment at  $10_1^+$ , namely the  $T = 0$   $1p1n$  aligned states from  $10_1^+$  to  $18_1^+$  above the  $gs$  band ( $0_1^+ - 8_1^+$ ). We can expect the existence of the  $T = 0$   $1p1n$  aligned states in  $^{70}\text{Se}$  and  $^{72}\text{Se}$  similar to  $^{66}\text{Ge}$  and  $^{68}\text{Ge}$ , but we made no calculations because of large dimensions.

### C. Odd- $J$ positive-parity yrast states

In the following three subsections, we investigate alignments in other yrast states with positive and negative parities ( $\pi = \pm$ ) of  $^{66}\text{Ge}$  and  $^{68}\text{Ge}$ .

The odd- $J$  positive-parity yrast states of  $^{66}\text{Ge}$  are interesting because of the cascade  $\Delta J = 1$  transitions on the  $11_1^+$  state [6] discussed in Sec. III B. For these odd- $J$  states, we show the expectation values of the spin and isospin of nucleons occupying the  $g_{9/2}$  orbit ( $J_{g_{9/2}}$  and  $T_{g_{9/2}}$ ) in the right panel of Fig. 9. The results and calculated nucleon occupation numbers in the four orbits show that a structural change takes place at  $11_1^+$  and the states  $11_1^+$ ,  $13_1^+$ ,  $15_1^+$ ,  $17_1^+$ , and  $19_1^+$  have the structure of the  $T = 0$ ,  $J = 9$   $1p1n$  alignment in the  $g_{9/2}$  orbit. The odd- $J$  states  $11_1^+$  to  $19_1^+$  and the even- $J$  states  $14_1^+$  to  $18_1^+$  have a common structure of the  $T = 0$ ,  $J = 9$   $1p1n$  alignment. Therefore we can understand the almost equivalent two  $J$ - $\omega$  graphs from  $13_1^+$  to  $19_1^+$  and from  $14_1^+$  to  $18_1^+$  in Fig. 4(a) (see the dotted and solid lines). It should be remembered that the  $12_1^+$  state resembles the  $1p1n$  aligned state rather than the  $2n$  aligned state. The cascade  $\Delta J = 1$  transitions  $15_1^+ \rightarrow 14_1^+ \rightarrow 13_1^+ \rightarrow 12_1^+ \rightarrow 11_1^+$  can be related to the common structure between the odd- $J$  and even- $J$  states in our model, which is in disagreement with the consideration of possible four-quasi-particle structure in Ref. [6]. The large value of

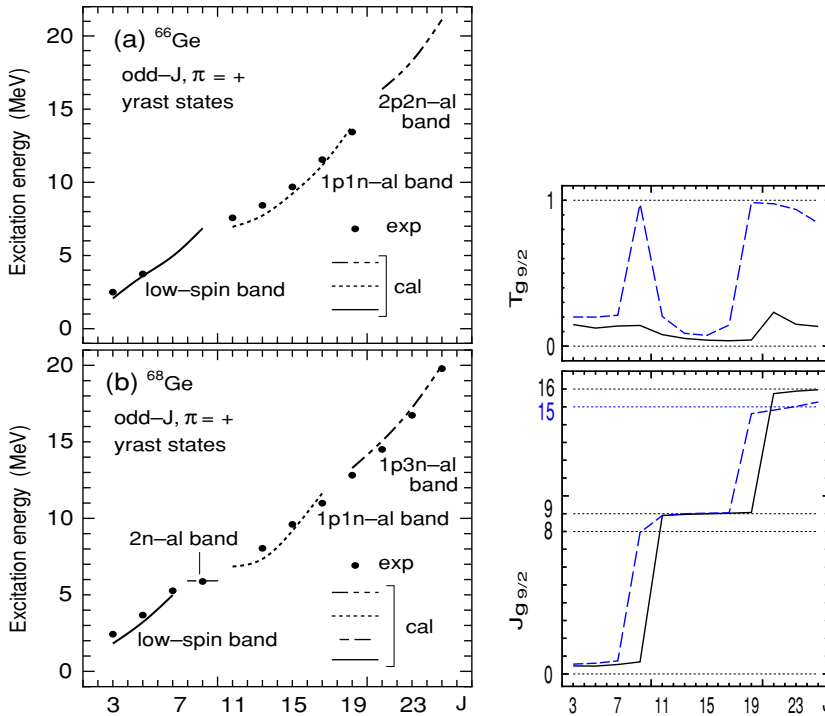


FIG. 9. (Color Online) Comparison of the calculated odd- $J$  positive-parity yrast states (curves) with the experimental ones (solid circles) for (a)  $^{66}\text{Ge}$  and (b)  $^{68}\text{Ge}$ . The expectation values  $J_{g_{9/2}}$  and  $T_{g_{9/2}}$  are shown in the right panel: solid lines for  $^{66}\text{Ge}$ ; dashed lines for  $^{68}\text{Ge}$ .

$B(M1 : 12_1^+ \rightarrow 11_1^+)$  in our calculation seems to be related to the strong mixing of the  $1p1n$  and  $2n$  aligned states at  $12_1^+$ .

It is notable that the  $T = 1, J = 8$   $2n$  aligned states do not become the yrast states when  $J = \text{odd}$  and  $\pi = +$  in  $^{66}\text{Ge}$ . This may be related to kinematic effects in the spin and isospin couplings. The calculation predicts that the yrast states  $21_1^+, 23_1^+$ , and  $25_1^+$  are the  $2p2n$  aligned states with  $J_{g_{9/2}} \approx 16$  and  $T_{g_{9/2}} \approx 0$ . We have the  $1p1n$  aligned band on  $11_1^+$  and the  $2p2n$  aligned band on  $21_1^+$  in addition to the low-spin band with no alignment, for the odd- $J$  positive-parity yrast states of  $^{66}\text{Ge}$ , as shown in Fig. 9(a). A good reproduction of the  $J$ - $\omega$  graph from  $13_1^+$  to  $17_1^+$  in Fig. 4(a) supports our classification.

For  $^{68}\text{Ge}$ , odd- $J$  positive-parity yrast states are experimentally observed up to  $25_1^+$ . Calculated results shown in the right panel of Fig. 9 indicate successive three types of particle aligned bands above the low-spin band with no alignment. They are the  $T = 1, J = 8$   $2n$  aligned band which has only one yrast state  $9_1^+$ , the  $T = 0, J = 9$   $1p1n$  aligned band from  $11_1^+$  to  $17_1^+$  and the one-proton-three-neutron ( $1p3n$ ) aligned band from  $19_1^+$  to  $25_1^+$ . Interestingly, the two excess neutrons in  $^{68}\text{Ge}$  as compared with  $^{66}\text{Ge}$  produce another type of particle alignment in the  $g_{9/2}$  orbit for the odd- $J$  positive-parity yrast states with  $J \geq 19$ . The  $1p3n$  aligned states have the combination of  $T = 1$   $2n$  pair and  $T = 0$   $pn$  pair in the  $g_{9/2}$  orbit which produces the spin  $J_{g_{9/2}} = 9/2^\pi + (9/2 + 7/2)^\nu = 15$  and the isospin  $T_{g_{9/2}} = 1$ . The calculation reproduces well the experimental  $J$ - $\omega$  graph for the  $J \geq 15$  states except  $17_1^+$ , as mentioned for Fig. 5(a). Thus, we have the four bands for the odd- $J$  positive-parity yrast states of  $^{68}\text{Ge}$ , as shown in the  $E_x$ - $J$  graph of Fig. 9(b). The calculation traces quite well the experimental footprints in Fig. 9(b).

#### D. Odd- $J$ negative-parity yrast states

There are sufficient data on odd- $J$  negative-parity yrast states of  $^{66}\text{Ge}$  and  $^{68}\text{Ge}$ . The negative-parity states have odd-number nucleons in the  $pf$  shell with  $\pi = -$  and hence at least one nucleon must occupy the  $g_{9/2}$  orbit in the even-mass Ge isotopes. This condition produces different structures from those of the positive-parity states in  $^{66}\text{Ge}$  and  $^{68}\text{Ge}$ .

Odd- $J$  negative-parity yrast states of  $^{66}\text{Ge}$  are experimentally observed up to tentative  $23_1^-$ . The right panel of Fig. 10 indicates that the low-spin states up to  $13_1^-$  have approximately one nucleon in the  $g_{9/2}$  orbit, giving the spin  $J_{g_{9/2}} \approx 9/2$  and the isospin  $T_{g_{9/2}} \approx 1/2$ . At  $15_1^-$ , one proton and two neutrons ( $1p2n$ ) align in the  $g_{9/2}$  orbit and produce the spin  $J_{g_{9/2}} = 9/2^\pi + (9/2 + 7/2)^\nu = 25/2$  and the isospin  $T_{g_{9/2}} = 1/2$ . The  $1p2n$  aligned band continues up to  $23_1^-$ , where the band terminates. The  $1p2n$  aligned states can be regarded as the  $T = 1$  aligned  $2n$  pair coupled with one proton and also as the  $T = 0$  aligned  $pn$  pair coupled with one neutron. We cannot distinguish the two types of coupling. Calculated proton and neutron occupation numbers in the  $g_{9/2}$  orbit predict that the next particle-aligned state is the two-proton-three-neutron ( $2p3n$ ) aligned state  $25_1^-$ . The sequence of the odd- $J$  negative-parity yrast states has two bands, the low-spin band, with one neutron in the  $g_{9/2}$  orbit, and the  $1p2n$  aligned band on  $15_1^-$ , which is shown in Fig. 10(a). The theoretical two bands nicely trace the experimental footprints.

Next we consider the odd- $J$  negative-parity yrast states of  $^{68}\text{Ge}$ . The right panel of Fig. 10 shows that the odd- $J$  negative-parity yrast states of  $^{68}\text{Ge}$  have essentially the same features as those of  $^{66}\text{Ge}$  with respect to the particle alignments in the  $g_{9/2}$  orbit. There are two bands, the low-spin band,

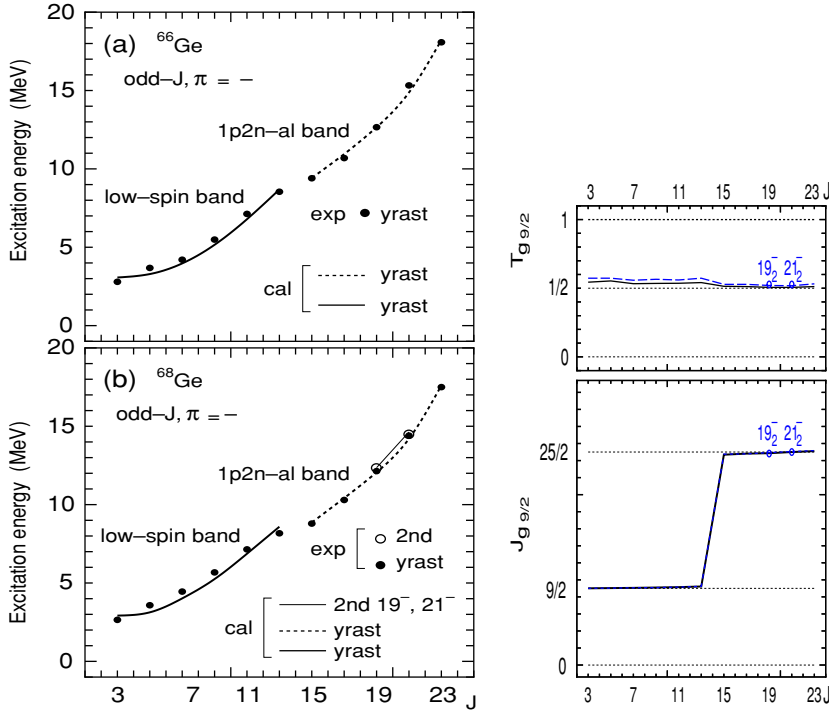


FIG. 10. (Color Online) Comparison of the calculated odd- $J$  negative-parity yrast states (curves) with the experimental ones (solid circles) for (a)  $^{66}\text{Ge}$  and (b)  $^{68}\text{Ge}$ . The expectation values  $J_{g_{9/2}}$  and  $T_{g_{9/2}}$  are shown in the right panel: solid lines for  $^{66}\text{Ge}$ ; dashed lines for  $^{68}\text{Ge}$ .

with one neutron in the  $g_{9/2}$  orbit, and the  $1p2n$  aligned band, which starts from  $15_1^-$  and terminates at  $23_1^-$ . In the  $1p2n$  aligned band, the three nucleons in the  $g_{9/2}$  orbit have  $J_{g_{9/2}} \approx 25/2$  and  $T_{g_{9/2}} \approx 1/2$ . We show the  $E_x$ - $J$  graph in Fig. 10(b). The agreement between theory and experiment is good especially for the  $1p2n$  aligned band on  $15_1^-$ . We have discussed the continuation of bands around  $J^\pi = 19^-$  and  $J^\pi = 21^-$  from the calculated  $B(E2)$  values in Sec. III B. Figure 10 shows that the  $19_2^-$  and  $21_2^-$  states also cause the  $1p2n$  alignment in the  $g_{9/2}$  orbit, which is consistent with Ref. [11], where these states are considered to be the states of the  $[01,2]$  configuration (one  $g_{9/2}$  proton and two  $g_{9/2}$  neutrons).

### E. Even- $J$ negative-parity yrast states of $^{68}\text{Ge}$

Even- $J$  negative-parity yrast states of  $^{68}\text{Ge}$  are experimentally observed up to  $J^\pi = 28^-$ . The right panel of Fig. 11 indicates that the even- $J$  negative-parity yrast states up to  $22_1^-$  have a nature similar to that of the odd- $J$  negative-parity yrast states up to  $23_1^-$  in  $^{68}\text{Ge}$ . The calculated high-spin states from  $14_1^-$  to  $22_1^-$  contain the aligned three nucleons ( $1p2n$ ) with  $J_{g_{9/2}} \approx 25/2$  and  $T_{g_{9/2}} \approx 1/2$  in the  $g_{9/2}$  orbit. This is in agreement with the calculated results of Ref. [11] that there are low-lying states ( $14_1^-$ ,  $16_1^-$ ,  $18_1^-$ ,  $20_1^-$ ,  $22_1^-$ ) of the  $[01,2]$  configuration. For the higher-spin states  $24_1^-$ ,  $26_1^-$ , and  $28_1^-$ , the right panel of Fig. 11 indicates the  $2p3n$  alignment coupled to  $J_{g_{9/2}} = (9/2 + 7/2)^\pi + (9/2 + 7/2 + 5/2)^\nu = 37/2$  and  $T_{g_{9/2}} = 1/2$  in the  $g_{9/2}$  orbit. These states are members of the  $2p3n$  aligned band. This assignment corresponds with that of the  $[02,3]$  configuration (two  $g_{9/2}$  protons and three  $g_{9/2}$  neutrons) for these states in Ref. [11]. This is supported by the calculated

$B(E2)$  values, a small value for the transition  $24_1^- \rightarrow 22_1^-$  (which shows discontinuity between the states  $22_1^-$  and  $24_1^-$ ) and large values for the transitions  $28_1^- \rightarrow 26_1^- \rightarrow 24_1^-$ . Calculated results show that there could be the  $2p3n$  aligned states with  $J = \text{odd}$ ,  $\pi = -$  above  $23_1^-$  in both  $^{66}\text{Ge}$  and  $^{68}\text{Ge}$ . We have three bands in the even- $J$  negative-parity yrast states of  $^{68}\text{Ge}$ , the low-spin band with one neutron in the  $g_{9/2}$  orbit, the  $1p2n$  aligned band on  $14_1^-$  and the  $2p3n$  aligned band on  $24_1^-$ , as shown in the  $E_x$ - $J$  graph of Fig. 11. The agreement between theory and experiment is not good for the low-spin band but is satisfactorily good for the  $1p2n$  and  $2p3n$  aligned bands.

### F. Dependence of the first band crossing on neutron number

We have seen the change of the first band crossing in  $^{66}\text{Ge}$  and  $^{68}\text{Ge}$ . The backbending takes place at  $10_1^+$  in  $^{66}\text{Ge}$  and  $8_1^+$  in  $^{68}\text{Ge}$ . Here we consider this backbending in the Ge isotopes, including  $^{64}\text{Ge}$  and  $^{70}\text{Ge}$ . We calculated energy levels of  $^{64}\text{Ge}$  and  $^{70}\text{Ge}$  with the same Hamiltonian as those for  $^{66}\text{Ge}$  and  $^{68}\text{Ge}$ . The force strengths in Eq. (4) are too strong for the  $gs$  band of the  $N = Z$  nucleus  $^{64}\text{Ge}$ , pushing up the energy levels as  $J$  increases. The present model is, however, good enough to discuss the band crossing near  $J = 8$ . The  $2n$  aligned states  $8^+$  and  $10^+$ , and the  $12^+$  state with dominant component of the  $1p1n$  alignment are denoted by the thick lines with the asterisks (as  $*8^+$ ) in Fig. 12(a).

In Fig. 12(a), whereas the experimental  $6_1^+$  state goes up gradually until  $^{68}\text{Ge}$  with  $N = 36$ , the  $8_1^+$  state reaches the peak at  $^{66}\text{Ge}$  with  $N = 34$  and goes down as  $N$  increases. The calculation indicates that the  $2n$  aligned  $8_1^+$  state does not intrude among the lowest three  $8^+$  states when  $N = 32$  but

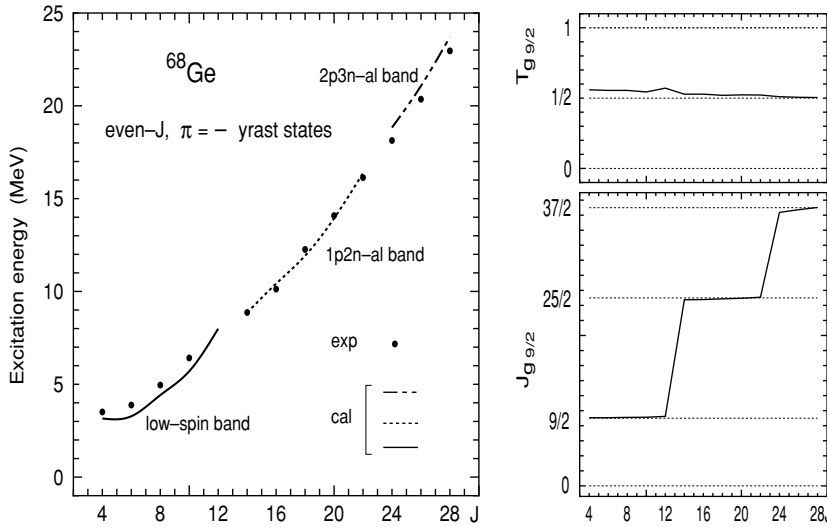


FIG. 11. Comparison of the calculated even- $J$  negative-parity states (curves) with the experimental ones (circles) for  $^{68}\text{Ge}$ . The expectation values  $J_{g9/2}$  and  $T_{g9/2}$  are shown in the right panel.

competes with the  $8^+$  member of the  $gs$  band when  $N = 34$  and becomes lower in energy than the latter when  $N \geq 36$ . This feature can be due to upward movement of the neutron Fermi level with the increase in the neutron number  $N$ . The approach of the Fermi level to the  $g_{9/2}$  orbit makes nucleons be easy to go into the  $g_{9/2}$  orbit and to get high spin by particle alignment.

The same behavior is observed in the Zn isotopes as shown in Fig. 12(b). We use the same force strengths for the Zn

isotopes with  $A = 62 - 68$ . The experimental  $6_1^+$  state goes up gradually until  $N = 36$ . The  $8_1^+$  state reaches the peak at  $N = 34$  and goes down as  $N$  increases. The change in the Zn isotopes shows a slight difference from that in the Ge isotopes. In  $^{64}\text{Zn}$  with  $N = 34$ , the  $2n$  aligned  $8^+$  state is lower than the  $8^+$  member of the  $gs$  band, but the backbending takes place at  $10_1^+$  like  $^{66}\text{Ge}$  with  $N = 34$ . The backbending at  $8_1^+$  is observed at  $N = 36$  also in the Zn isotopes. (The same behavior of the  $8_1^+$  state is seen also in the experimental level schemes of Se isotopes.) The common behavior depending on the neutron number supports our conclusion that the first band crossing (backbending) at  $8_1^+$  is caused by the  $2n$  alignment in the  $g_{9/2}$  orbit.

### V. NUCLEAR SHAPES OF GE ISOTOPES

The nuclear shape or the coexistence of oblate and prolate shapes has been a hot topic in nuclei around Ge isotopes [6,19–23]. For instance, the VAMPIR gave positive (oblate)  $Q$  moments to the  $gs$  band and negative (prolate)  $Q$  moments to the second low-spin band in  $^{68}\text{Ge}$  [13–15]. The other recent calculations [6,21] also yielded the deepest minimum for an oblate shape and the next minima for prolate shapes in  $^{66}\text{Ge}$  and  $^{68}\text{Ge}$  and predicted shape coexistence and  $\gamma$  softness. The present shell-model calculations give negative  $Q$  moments for the states of the  $gs$  band and other states, except the  $2_2^+$  and  $4_3^+$  states of  $^{66}\text{Ge}$  and the  $2_2^+$ ,  $4_3^+$ , and  $6_2^+$  states of  $^{68}\text{Ge}$ , which have positive  $Q$  moments. This means that prolate shape is favored for low-lying states of both  $^{66,68}\text{Ge}$ . Our results predict a different picture in shape.

Figure 13 suggests a gradual decrease of the prolate (oblate) deformation of the  $2_1^+$  ( $2_2^+$ ) state from  $^{66}\text{Ge}$  to  $^{68}\text{Ge}$ . The calculation for  $^{64}\text{Ge}$  yields negative  $Q$  moments for the  $gs$  band and exceptionally yields a positive  $Q$  moment for the  $2_2^+$  state, which is similar to the results for  $^{66}\text{Ge}$  and  $^{68}\text{Ge}$ . However, the  $Q$  moment of the  $2_1^+$  state [ $Q(2_1^+)$ ] has not been experimentally observed for  $^{66}\text{Ge}$  and  $^{68}\text{Ge}$  yet. In  $^{70}\text{Ge}$ , on the contrary, the  $2_1^+$  and  $4_1^+$  states have small positive  $Q$  moments, whereas the  $2_2^+$  state has a small negative  $Q$  moment. The

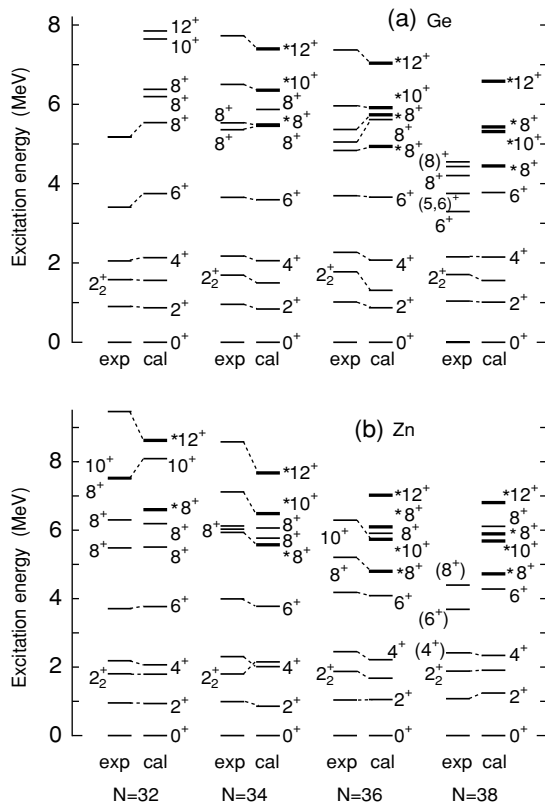


FIG. 12. Changes of the low-energy levels in the (a) Ge and (b) Zn isotopes. The  $2n$  and  $1p1n$  aligned states (thick lines) are distinguished with the asterisks from the members of the  $gs$  band.

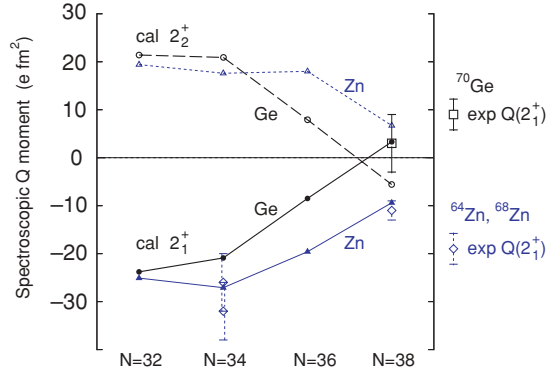


FIG. 13. (Color Online) Calculated  $Q$  moments for the Ge isotopes (solid and open circles) and Zn isotopes (solid and open triangles) compared with the experimental ones.

$Q(2_1^+)$  is measured for  $^{70}\text{Ge}$ . This shell-model value is in good agreement with the experimental value. The present result for  $Q(2_1^+)$  is better than those of Refs. [13–15].

For  $^{64}\text{Zn}$  and  $^{68}\text{Zn}$ , there are two experimental data on  $Q(2_1^+)$ . Then we calculated  $Q$  moments for the Zn isotopes from  $^{62}\text{Zn}$  to  $^{68}\text{Zn}$ , which are shown in Fig. 13. The present shell-model also well reproduces these experimental  $Q(2_1^+)$  values of  $^{64}\text{Zn}$  and  $^{68}\text{Zn}$ . Similar decreases of the prolate and oblate deformations of the  $2_1^+$  and  $2_2^+$  states from  $^{64}\text{Zn}$  to  $^{68}\text{Zn}$  are also seen. There seems to be a trend that the prolate (oblate) shape of the  $2_1^+$  ( $2_2^+$ ) state tends toward the oblate (prolate) shape when the neutron number goes over  $N = 34$ . This trend is clearer in the Ge isotopes than in the Zn isotopes.

Next we investigate further the nuclear shapes of the Ge isotopes and their triaxiality by PES within the present shell-model framework [35,36]. We consider the modified Hamiltonian with the following quadratic terms of quadrupole moment  $q_M$  and spin  $J$ :

$$H' = H + c_1 \sum_M (\langle Q_{2M} \rangle - q_M)^2 + c_2 [ \langle J_x \rangle - \sqrt{J(J+1)} ]^2, \quad (5)$$

where  $J_x$  denotes the  $x$  component of the angular momentum operator and  $q_0 = \sqrt{5/4\pi} q \cos \gamma$ ,  $q_{\pm 1} = 0$ , and  $q_{\pm 2} = \sqrt{5/8\pi} q \sin \gamma$ . We consider the ground state with  $J = 0$  in Eq. (5). The parameters  $c_1$  and  $c_2$  are taken so as to achieve convergence of the iteration of the gradient method. By solving the CHF equation with the above Hamiltonian, we obtain the potential energy surface  $\langle q, \gamma | H | q, \gamma \rangle$  in the  $q$ - $\gamma$  plane.

In Fig. 14(a) for  $^{66}\text{Ge}$ , the energy surface has a minimum near  $q \approx 56 \text{ fm}^2$  and  $\gamma \approx 0^\circ$ , suggesting an axially symmetric prolate deformation with  $\beta \approx 0.2$ . This value  $\beta \approx 0.2$ , which is consistent with the calculated  $B(E2)$  value  $B(E2: 2_1^+ \rightarrow 0_1^+) \approx 281 e^2 \text{ fm}^4$  on the assumption of the axial symmetry, corresponds with previous predictions  $\beta \approx 0.2 - 0.22$  [6,22]. The energy surface in Fig. 14(a), however, displays a valley along the  $\gamma$  direction, which means  $\gamma$  softness of  $^{66}\text{Ge}$  like  $^{64}\text{Ge}$  (see Ref. [34]). The energy surface for  $^{68}\text{Ge}$  indicates a triaxial

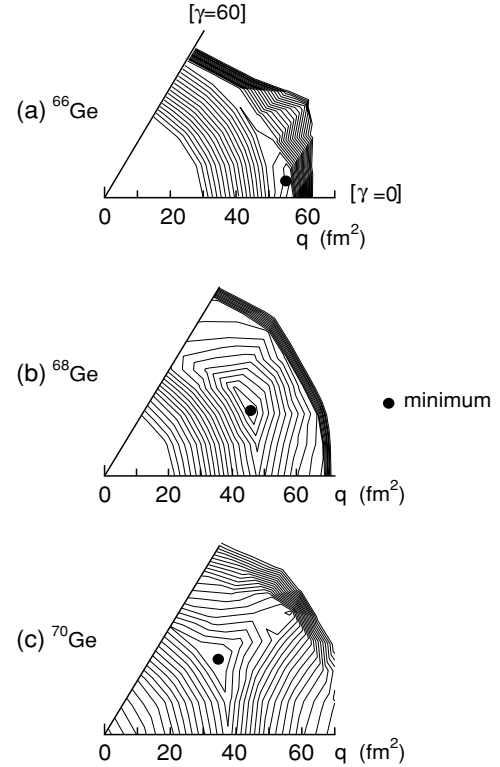


FIG. 14. The energy surface  $\langle q, \gamma | H | q, \gamma \rangle$  in the  $q$ - $\gamma$  plane ( $0^\circ \leq \gamma \leq 60^\circ$ ) plotted with contours, for (a)  $^{66}\text{Ge}$ , (b)  $^{68}\text{Ge}$ , and (c)  $^{70}\text{Ge}$ . The contour lines denote the increase of energy from the minimum point.

deformation in Fig. 14(b). The minimum is near  $q \approx 50 \text{ fm}^2$  and  $\gamma \lesssim 30^\circ$  in the  $q$ - $\gamma$  plane. This seems to be consistent with the small negative value of  $Q(2_1^+)$  obtained by the shell-model calculation, from the relation  $Q \propto -q \cos(3\gamma)$  in the Davydov model. The energy surface for  $^{70}\text{Ge}$  also shows a triaxial deformation in Fig. 14(c). The minimum near  $q \approx 45 \text{ fm}^2$  and  $\gamma \gtrsim 30^\circ$  in the  $q$ - $\gamma$  plane corresponds to the small positive value of the experimental  $Q$  moment  $Q(2_1^+)$ .

The PES analysis thus supports the shape change depending on the neutron number from  $^{66}\text{Ge}$  to  $^{70}\text{Ge}$  as the movement along the  $\gamma$  direction (crossing the  $\gamma = 30^\circ$  border) with a gradual decrease of quadrupole deformation in the  $q$ - $\gamma$  plane. A similar trend is seen in PESs of the Zn isotopes from  $^{64}\text{Zn}$  to  $^{68}\text{Zn}$ . The PES analysis for  $^{66}\text{Ge}$  and  $^{68}\text{Ge}$  gives a different picture in contrast with the TRS calculations [6].

## VI. SUMMARY

We have investigated the structure of  $^{66}\text{Ge}$  and  $^{68}\text{Ge}$ , by carrying out large-scale shell-model calculations with the extended  $P + QQ$  Hamiltonian in the configuration space ( $2p_{3/2}, 1f_{5/2}, 2p_{1/2}, 1g_{9/2}$ ). The shell model reproduces excellently the energy levels of  $^{66}\text{Ge}$  and  $^{68}\text{Ge}$  (and satisfactorily those of  $^{64,65,67,70}\text{Ge}$ ). The model explains well the graphs of spin versus angular frequency for the positive- and

negative-parity yrast states with even  $J$  and odd  $J$ . The calculated  $B(E2)$  values are basically consistent with the band schemes assigned by  $\gamma$  transitions in the experiments [6,11].

To analyze the structure, we calculated the proton and neutron occupation numbers in the four orbits, the expectation values of the spin and isospin of nucleons in the  $pf$  shell ( $2p_{3/2}$ ,  $1f_{5/2}$ ,  $2p_{1/2}$ ) and in the  $g_{9/2}$  orbit, and the spectroscopic  $Q$  moment. The analysis has clarified that the structural changes in the four sequences of the positive- and negative-parity yrast states with even  $J$  and odd  $J$  are caused by various types of particle alignments in the  $g_{9/2}$  orbit as follows.

- (a)  $^{66}\text{Ge}$ : (1) The even- $J$ ,  $\pi = +$  sequence has the four bands up to  $26_1^+$ : the  $gs$  band, the  $2n$  aligned band, the  $1p1n$  aligned band, and the  $2p2n$  aligned band. (2) The odd- $J$ ,  $\pi = +$  sequence has the three bands up to  $25_1^+$ : the low-spin band, the  $1p1n$  aligned band, and the  $2p2n$  aligned band. (3) The odd- $J$ ,  $\pi = -$  sequence has the two bands up to  $23_1^-$ : the low-spin band and the  $1p2n$  aligned band.
- (b)  $^{68}\text{Ge}$ : (1) The even- $J$ ,  $\pi = +$  sequence has the four bands up to  $26_1^+$ : the  $gs$  band, the  $2n$  aligned band, the  $1p1n$  aligned band, and the  $2p2n$  aligned band. (2) The odd- $J$ ,  $\pi = +$  sequence has the four bands up to  $25_1^+$ : the low-spin band, the  $2n$  aligned state, the  $1p1n$  aligned band, and the  $1p3n$  aligned band. (3) The odd- $J$ ,  $\pi = -$  sequence has the two bands up to  $23_1^-$ : the low-spin band and the  $1p2n$  aligned band. (4) The even- $J$ ,  $\pi = -$  sequence has

the three bands up to  $28_1^-$ : the low-spin band, the  $1p2n$  aligned band, and the  $2p3n$  aligned band.

We have also looked into the nuclear shapes of the Ge isotopes at low energy where no particle alignment takes place. The calculations have made the following predictions. The  $2_1^+$  state has a negative  $Q$  moment in  $^{66}\text{Ge}$  and  $^{68}\text{Ge}$  and has a positive  $Q$  moment in  $^{70}\text{Ge}$ , whereas the  $2_2^+$  state has an opposite sign of the  $Q$  moment against the  $2_1^+$  state in these nuclei. The prolate (oblate) deformation of the  $2_1^+$  ( $2_2^+$ ) state decreases from  $^{66}\text{Ge}$  to  $^{68}\text{Ge}$ . The PES analysis indicates the shape change depending on the neutron number as the movement along the  $\gamma$  direction (crossing the  $\gamma = 30^\circ$  border) with a gradual decrease of quadrupole deformation in the  $q$ - $\gamma$  plane. The ground state of  $^{66}\text{Ge}$  is prolate and those of  $^{68}\text{Ge}$  and  $^{70}\text{Ge}$  are triaxial. The predictions are supported by the agreement between the calculated and experimental  $Q$  moments [ $Q(2_1^+)$ ] in  $^{70}\text{Ge}$ ,  $^{64}\text{Zn}$ , and  $^{68}\text{Zn}$ .

We have shown only the energy levels for the odd-mass nuclei  $^{65}\text{Ge}$  and  $^{67}\text{Ge}$ . The present model predicts the  $1p1n$  alignment in these nuclei. We shall discuss a unique structure of  $N \approx Z$  odd-mass nuclei in this region elsewhere.

#### ACKNOWLEDGMENTS

This work was supported by the Grant-in-Aid of the Promotion and Mutual Aid Corporation for Private Universities of Japan in 2003 and 2004.

- 
- [1] E. Nolte, Y. Shida, W. Kutschera, R. Prestele, and H. Morinaga, *Z. Phys.* **268**, 267 (1974).
- [2] L. Cleenmann, J. Eberth, W. Neumann, W. Wiehl, and V. Zobel, *Nucl. Phys.* **A334**, 157 (1980).
- [3] R. Soundranayagam, R. B. Piercey, A. V. Ramayya, J. H. Hamilton, A. Y. Ahmed, H. Yamada, C. F. Maguire, G. L. Bomar, R. L. Robinson, and H. J. Kim, *Phys. Rev. C* **25**, 1575 (1982).
- [4] A. Boucenna, L. Kraus, I. Linck, and Tsan Ung Chan, *Phys. Rev. C* **42**, 1297 (1990).
- [5] U. Hermkens, F. Becker, J. Eberth, S. Freund, T. Mylaeus, S. Skoda, W. Teichert, and A.v.d. Werth, *Z. Phys. A* **343**, 371 (1992).
- [6] E. A. Stefanova *et al.*, *Phys. Rev. C* **67**, 054319 (2003).
- [7] R. C. Pardo, C. N. Davids, M. J. Murphy, E. B. Norman, and L. A. Parks, *Phys. Rev. C* **15**, 1811 (1977).
- [8] A. P. de Lima *et al.*, *Phys. Rev. C* **23**, 213 (1981).
- [9] L. Chaturvedi *et al.*, *Phys. Rev. C* **43**, 2541 (1991).
- [10] L. Chaturvedi *et al.*, *Int. J. Mod. Phys. E* **5**, 1565 (1996).
- [11] D. Ward *et al.*, *Phys. Rev. C* **63**, 014301 (2001).
- [12] M. E. Barclay, *J. Phys. G* **12**, L295 (1986).
- [13] A. Petrovici, K. W. Schmid, F. Gümer, and A. Faessler, *Nucl. Phys.* **A483**, 317 (1988).
- [14] A. Petrovici, K. W. Schmid, F. Gümer, and A. Faessler, *Nucl. Phys.* **A504**, 277 (1989).
- [15] A. Petrovici, K. W. Schmid, F. Gümer, and A. Faessler, *Nucl. Phys.* **A517**, 108 (1990).
- [16] S. T. Hsieh, H. C. Chiang, and Der-San Chuu, *Phys. Rev. C* **46**, 195 (1992).
- [17] Der-San Chuu, S. T. Hsieh, and H. C. Chiang, *Phys. Rev. C* **47**, 183 (1993).
- [18] J. P. Elliott, J. A. Evans, V. S. Lac, and G. L. Long, *Nucl. Phys.* **A609**, 1 (1996).
- [19] R. Bengtsson, P. Möller, J. R. Nix, and J. Zhang, *Phys. Scr.* **29**, 402 (1984).
- [20] W. Nazarewicz, J. Dudek, R. Bengtsson, T. Bengtsson, and I. Ragnarsson, *Nucl. Phys.* **A435**, 397 (1985).
- [21] P. Sarriguren, E. Moya de Guerra, and A. Escuderos, *Nucl. Phys.* **A658**, 13 (1999).
- [22] P. J. Ennis, C. J. Lister, W. Gellately, H. G. Price, B. J. Varley, P. A. Butler, T. Hoare, S. Cwiok, and W. Nazarewicz, *Nucl. Phys.* **A535**, 392 (1991).
- [23] M. Yamagami, K. Matsuyanagi, and M. Matsuo, *Nucl. Phys.* **A693**, 579 (2001).
- [24] K. Kaneko, M. Hasegawa, and T. Mizusaki, *Phys. Rev. C* **66**, 051306(R) (2002).
- [25] M. Hasegawa and K. Kaneko, *Phys. Rev. C* **59**, 1449 (1999).
- [26] M. Hasegawa, K. Kaneko, and S. Tazaki, *Nucl. Phys.* **A674**, 411 (2000); **688**, 765 (2001); *Prog. Theor. Phys.* **107**, 731 (2002).
- [27] T. Mizusaki, *RIKEN Accel. Prog. Rep.* **33**, 14 (2000).
- [28] M. Hasegawa, K. Kaneko, and T. Mizusaki, *Phys. Rev. C* **70**, 031301(R) (2004).
- [29] D. Rudolph *et al.*, *Eur. Phys. J. A* **6**, 377 (1999).

- [30] A. Juodagalvis and S. Åberg, Nucl. Phys. **A683**, 206 (2001).
- [31] Yang Sun, Jing-ye Zhang, M. Guidry, Jie Meng, and Soojae Im, Phys. Rev. C **62**, 021601(R) (2000).
- [32] <http://www.nndc.bnl.gov/nndc/ensdf>.
- [33] M. Hasegawa, K. Kaneko, T. Mizusaki, and S. Tazaki, Phys. Rev. C **69**, 034324 (2004).
- [34] K. Kaneko, M. Hasegawa, and T. Mizusaki, Phys. Rev. C **70**, 051301(R) (2004).
- [35] T. Mizusaki, T. Otsuka, Y. Utsuno, M. Honma, and T. Sebe, Phys. Rev. C **59**, 1846(R) (1999).
- [36] K. Hara, Yang Sun, and T. Mizusaki, Phys. Rev. Lett. **83**, 1922 (1999).